

## Numerical Simulation of High Speed Rotating Waterjet Flow Field in a Semi Enclosed Vacuum Chamber

Haojun Peng<sup>1,\*</sup> and Ping Zhang<sup>2</sup>

**Abstract:** In this paper, a three dimension model is built according to real surface cleaner in airport runway rubber mark cleaning vehicle and numerical simulation of this model is carried out using Ansys Fluent software. After comparison and analysis of the flow fields between high speed rotating waterjet and static waterjet formerly studied by other researchers, the influences of different standoff distances from nozzle outlet to runway surface and rotation speeds on rubber mark cleaning effect are simulated and analyzed. Results show the optimal operation parameters for the simulated model and quantitative advices are given for design, manufacture and operation of the airport runway rubber mark cleaning vehicle.

**Keywords:** Airport runway cleaning, surface cleaner, rotating flow field, numerical simulation.

### 1 Introduction

High pressure waterjet technology is often used to clean the rubber mark caused by severe friction between airplane tires and airport runway surface during landing and recover runway friction coefficient. In recent years, this technology is also gradually spread out to municipal engineering such as road cleaning and mark line removing. Whatever the application is, high pressure waterjet surface cleaner is one of the indispensable and important components. As shown in Fig. 1, its body is a 304 stainless steel shell with a high pressure rotary coupling installed on top center, at whose end 4 spraying lances are installed with 90° interval angle. Each spraying lance has a high pressure nozzle mounted at the end. During cleaning, the spraying lances are driven to rotate, cooperating with the forward moving of whole equipment and fulfilling the surface cleaning process. On top of the shell, there is a suction pipe. All solid particles cleaned and waste water will be sucked out of the shell and collected to treat. Between lower end of the shell and ground, there is a small gap to let air flowing in. But for consideration of decreasing vacuum pump's power consumption, this gap is usually wrapped by two or three layers of nylon brush strip to prevent excessive leakage.

---

<sup>1</sup> School of Mechanical Engineering, Hefei University of Technology, Hefei, Anhui, China

<sup>2</sup> School of Mechanical and Electrical Engineering, Anhui Water Conservancy Technical College, Hefei, Anhui, China

\* Corresponding author: Haojun Peng. Email: waterjet@sina.com

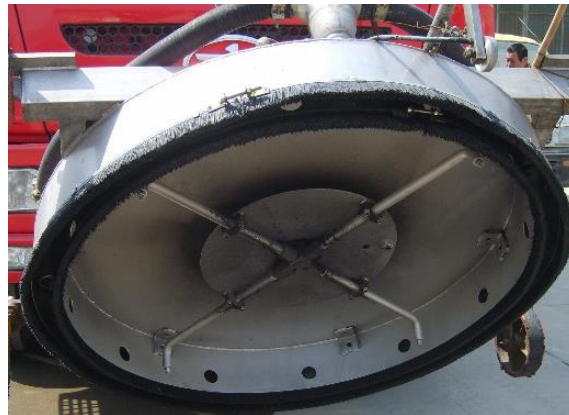


**Figure 1:** Structure of surface cleaner

Nowadays, working parameters of most surface cleaners manufactured by different producers are normally chosen according to former experiences or similar products. Fewer of them are selected on the basis of quantitative analysis. These working conditions without optimization inevitably lead to conservative parameters design, increasing size of whole equipment and manufacturing costs. So it is urgent to simulate the inner flow field of surface cleaner and optimize these operation parameters accordingly to reduce its cost by choosing appropriate parameters while maximizing its performance.

## 2 Description of problem

The operation conditions of typical airport runway mark cleaning vehicle are: 70 MPa pressure and 70 L/min flow rate for its high pressure waterjet system; 15~18 m<sup>3</sup>/min air flow rate, -0.015~-0.03 MPa relative pressure vacuum degree and 37~45 kW power for its vacuum suction system.

When water flows out of nozzle at 70 MPa, the jet's speed at nozzle outlet reaches about 374.6 m/s and its Reynold number is about 370149. The momentum and energy interchange between this severely turbulent high speed waterjet and ambient atmosphere, combining with the air intake flow from lower gap and the tangential force generated by high speed rotation, makes the flow field within surface cleaner become a complicated multiphase turbulence flow field. Its characteristics can only be studied through numeric simulation.

Labus et al. [Labus (1995); Summers (1995)] all pointed out that the basic waterjet structure can be divided into three parts, which were initial section, basic section and dissipation section. They also stated that the initial section was normally used for waterjet cutting, the basic section was used for cleaning, dust removing and surface polishing, while the dissipation section can only be used for dust elimination. Tikhomirov, et al. [Tikhomirov, Babanin, Petukhov et al. (1992)] discussed the interaction procedure between waterjet droplet and target material. They measured the relation between jet pressure and jet striking time at the center of jet impacting area and summarized the

relationship of jet's striking force on target material with standoff distance during waterjet cutting with different working pressures and nozzle sizes on the basis of experiment data. Sun [Sun (1992)] gave the empirical formula for calculating dynamic pressure at waterjet axle center and dynamic pressure distribution at different section faces.

Li et al. [Li, Wang, Zhu et al. (2013)] calculated and simulated the impact procedure of 350~700 m/s ultra-high speed waterjet onto high strength steel plate during abrasive waterjet rust removing process. They researched the transferring procedure of impact energy to ductile material and the relationships of erosion cavity's volume and material removing efficiency to different impacting variables and yield strength of target material. Research results of Welker et al. [Welker, Nagarajan and Newberg (2005)] show that the elimination course of solid particles adhered on material surface is mainly related to shear stress generated by jet impacting onto target material. Leu et al. [Leu, Meng, Geskin et al. (1998)] built a mathematic model for waterjet cleaning process. Highlight of their research is that they demonstrated the cleaning effect can be emerged only when the shear stress generated by water droplet striking onto target is equal to or more than the fatigue limit of target material during waterjet impacting on target surface.

Yang et al. [Yang, Zhou and Liu (2008)] used numeric simulation and calculated speed field and pressure field of water jet in atmosphere produced by several nozzles in different working conditions. And there are many similar researches can be found. But fewer research about the high speed rotating waterjet flow field in semi enclosed vacuum chamber in surface cleaner can be seen. The most similar and unique research was conducted by Li et al. [Li, Xue and Zhou (2007)] in their study on ultra-high pressure waterjet rust removing. They estimated the waterjet speed distribution under 200 MPa pressure, gave the pressure and flow speed distribution on jet striking surface, proposed the relationship between striking force on target surface and standoff distance and discussed the optimization of waterjet working parameters. But regretfully, they assumed the rotation speed of spraying lances was zero and ignored the influence of waterjet rotation on cleaning effect, which was far deviated from actual equipment and cleaning process.

### **3 Determination of calculation model**

Fig. 2 shows the geometry model built according to real surface cleaner. Its main body is a cylindrical shell, which has a 1050 mm diameter and 185 mm height. A 6 mm air intake gap is located between lower end of the shell and ground. The bias welded  $\varnothing$  100 mm cylindrical pipe installed on top is the intake of vacuum suction system. Four  $\varnothing$  22 mm outer diameter high pressure spraying lances and mm cylindrical nozzles are mounted symmetrically at the center on top shell plate. Mesh using tetrahedral element is shown in Fig. 3, where the meshes in inner body and on bottom surface are hidden for clear demonstration.

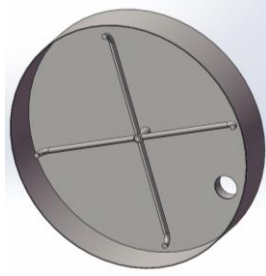


**Figure 2:** Geometry model

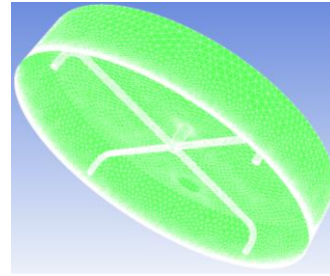
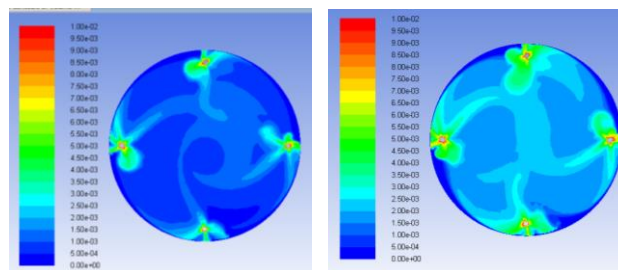


**Figure 3:** Mesh

### 3.1 Selection of turbulence model

The most commonly used turbulence models in Fluent Software are  $k-\varepsilon$  model and  $k-\omega$  model. Standard  $k-\varepsilon$  model is used more widely for its higher stability, economy and calculation accuracy. It is fit for simulation of high Reynold number turbulence. But its basic assumption is that the eddy viscosity of turbulence is isotropic, which makes it unsuitable for flow simulation with higher aeolotropism, let alone appropriate wall function should be adopted for successful application. On the other hand, Standard  $k-\omega$  model is specially developed for flow simulation with higher pressure gradient. Compared with  $k-\varepsilon$  model,  $k-\omega$  model can simulate flow field near wall more precisely and is suitable for simulation of free shear turbulence, jet, turbulence adhered to boundary layer and flow restricted by wall.

In this simulation, the high speed jet flows out of nozzle orifice in high Reynold number turbulent state and exchanges momentum and energy severely with ambient atmosphere. Moreover, to enlarge cleaning area and improve cleaning efficiency to maximum extent, distance between nozzle and shell wall is set to be small, combined with the bent trajectory of jet in air caused by high speed rotated spraying lance and high speed air flow from air intake. All these factors make the flow field in vacuum shell of surface cleaner cannot meet the isotropic eddy viscosity assumption. So the  $k-\omega$  model is preferable. This conclusion is testified in initial simulation, which is shown in Fig. 4.



a.  $k-\varepsilon$  Model Simulation      b.  $k-\omega$  Model Simulation

**Figure 4:** Phase distribution in percent (%) on ground in vacuum chamber simulated by different turbulence model

As shown in Fig. 4, both calculations using  $k$ - $\varepsilon$  model and  $k$ - $\omega$  model with same meshing and initial conditions demonstrate convergence. But for distribution of water phase on ground in vacuum chamber, the result gained from  $k$ - $\omega$  model is much more similar to that observed in real test, which shows a more even mixing of water and air phases. Compared with  $k$ - $\omega$  model, the interfaces of water and air phases in  $k$ - $\varepsilon$  model are too clear to reflect real flow field in vacuum chamber, which shows poor applicability.

$k$  equation and  $\omega$  equation of SST  $k$ - $\omega$  model are listed as following:

$$\frac{\partial(\rho k)}{\partial t} + \frac{\partial(\rho k u_i)}{\partial x_i} = \frac{\partial}{\partial x_j} \left( \Gamma_k \frac{\partial k}{\partial x_j} \right) + G_k - Y_k + S_k \quad (1)$$

$$\frac{\partial(\rho \omega)}{\partial t} + \frac{\partial(\rho \omega u_i)}{\partial x_i} = \frac{\partial}{\partial x_j} \left( \Gamma_\omega \frac{\partial \omega}{\partial x_j} \right) + G_\omega - Y_\omega + D_\omega + S_\omega \quad (2)$$

In Eq. (1) and Eq. (2),  $G_k$  and  $G_\omega$  represents the generation of turbulent kinetic energy due to mean velocity gradients and generation of  $\omega$ .  $\Gamma_k$  and  $\Gamma_\omega$  represents the effective diffusivity of  $k$  and  $\omega$  respectively.  $Y_k$  and  $Y_\omega$  represents the dissipation of  $k$  and  $\omega$  due to turbulence respectively.  $D_\omega$  is the cross diffusion term and is defined as following,

$$D_\omega = 2(1 - F_t) \rho \sigma_{\omega,2} \frac{1}{\omega} \frac{\partial k}{\partial x_j} \frac{\partial \omega}{\partial x_j} \quad (3)$$

where the blending function  $F_t$  is defined as  $F_t = \tanh(\arg_1^4)$

$$\text{where } \arg_1^4 = \min \left[ \max \left( \frac{\sqrt{k}}{C_\mu \omega y}, \frac{500\nu}{y^2 \omega} \right), \frac{4\rho\sigma_{\omega,2}k}{CD_{k\omega}y^2} \right]$$

Here  $y$  is defined as the normal distance to wall and  $CD_{k\omega}$  is the positive portion of the cross diffusion term [Kummitha (2016)].

### **3.2 Selection of multiphase flow model**

This simulation is an air-water two-phase flow. Two types four kinds multiphase models in Fluent can be used, which are DPM model (Discrete Phase Model), VOF (Volume of Fluid) model, Mix (Mixture) model and Euler Model.

In these four models, the DPM model has an important assumption that the particle phase is very thin, so that the interaction between particles and influence of particle volume fraction on continuous phase can all be ignored. This assumption requires that the discrete phase has a volume fraction less than 10~12%. VOF model is a surface tracking method under fixed Euler meshing and is normally used for interface simulation for two or more mutually insoluble fluids, which has no interweaving between phases. The Euler model regards continuous phase and disperse phase as a continuous unit, builds momentum equation and continuity equation for each phase and solves these equations through coupling of pressure and exchange coefficient between phases. The Mix model is a simplified multiphase model, which uses single fluid equations to simulate multiphase flow with different phase speed.

For simulation in this paper, the vacuum shell of surface cleaner is filled with both air and large quantity tiny water droplets generated by high speed waterjet impacting on ground. Volume fraction proportions of air phase and water phase is near 1:1. And more, two phases are mixed thoroughly by their turbulent velocity and sucked air and no distinguishable and fixed interface exists. Considering above reasons and calculation conditions, speed and convergence, the Mix model is chosen as the final adopted multiphase flow model.

The continuity equation of Mix model is given as following,

$$\frac{\partial}{\partial t}(\rho m) + \nabla \cdot (\rho_m \vec{v}_m) = \dot{m} \quad (4)$$

Here,  $\vec{v}_m$  is the mass-averaged velocity given by  $\vec{v}_m = \frac{\sum_{k=1}^n \alpha_k \rho_k \vec{v}_k}{\rho_m}$ , and  $\rho_m$  is the mixture

density given by  $\rho_m = \sum_{k=1}^n \alpha_k \rho_k$ . In above expressions,  $\alpha_k$  is the volume fraction of phase  $k$ .

The momentum equation of Mix model is given as following,

$$\begin{aligned} \frac{\partial}{\partial t}(\rho_m \vec{v}_m) + \nabla \cdot (\rho_m \vec{v}_m \vec{v}_m) = & -\nabla p + \nabla \cdot [\mu_m (\nabla \vec{v}_m + \nabla \vec{v}_m^T)] \\ & + \rho m \vec{g} + \vec{F} + \nabla \cdot \left( \sum_{k=1}^n \alpha_k \rho_k \vec{v}_{dr,k} \vec{v}_{dr,k} \right) \end{aligned} \quad (5)$$

where  $n$  is number of phases;  $\vec{F}$  is the volume force;  $\mu_m$  is the mixture viscosity and given by  $\mu_m = \sum_{k=1}^n \alpha_k \mu_k$ ;  $\vec{v}_{dr,k}$  is the drift velocity of phase  $k$  and calculated by  $\vec{v}_{dr,k} = \vec{v}_k - \vec{v}_m$ .

### 3.3 Boundary conditions

In most actual cleaning equipment, the high pressure rotary coupling and spraying lances are driven by motor, there is no need to use tangential component of jet reactive thrust as driving power, and their spraying lances are installed vertically to ground. Although there are some cleaners that have obliquely installed spraying lances, but their proportion is very small. So only the vertical jet is considered in this simulation.

Most nozzle installed at the end of each spraying lance is a flat fan nozzle or a group of fine cylindrical hole nozzles to enlarge cleaning path and decrease the possibility of doing harm to runway surface. To simplifying simulation, no matter what kind of the nozzle is used, it is transferred to an equivalent nozzle with cylindrical hole. Outlets of 4 nozzles are set to be pressure inlet with normal working pressure of 70 MPa. Suction pipe is set to be pressure outlet with absolute pressure of 0.08 MPa (relative pressure -0.02 MPa). The air intake between lower end of shell and ground is speed inlet, whose value is calculated according to real vacuum pump typical rotation speed and set vacuum degree.

4 Results and Discussion

4.1 Transformation of flow field

Outlet of waterjet nozzle in this simulation is a cylindrical hole. Theoretically speaking, a waterjet sprayed into surrounding open space from cylindrical outlet without any air disturbance is a solid cone which is symmetrical to outlet axle. But in actual equipment, each surface cleaner is equipped with a stainless steel shell to reduce noise level and collect cleaned waste. At the meantime, the spraying lance is always designed to be as long as possible to enlarge cleaning area in single rotation to maximum extent. All these considerations make the distance between shell wall and nozzle relatively small, which leads to deformation of inner flow field in cleaner chamber. Under the joint actions of intake air and suction flow blowing, wall-attachment effect in small space between jet outlet and shell wall and high speed rotation of spraying lance, flow field of each nozzle cannot maintain axisymmetric shape when flowing freely and without any obstruction. It should be changed into an asymmetric structure in which obvious effects of wall-attachment and rotation can be seen.

Fig. 5 shows the velocity field and phase distribution (water phase percentage) on section plane cut through spraying lance axle under 800 rpm rotation speed and different standoff distance.

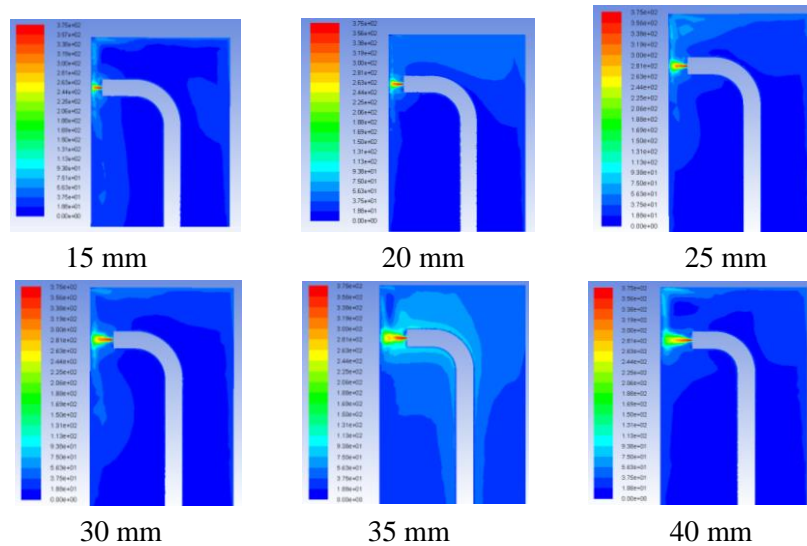
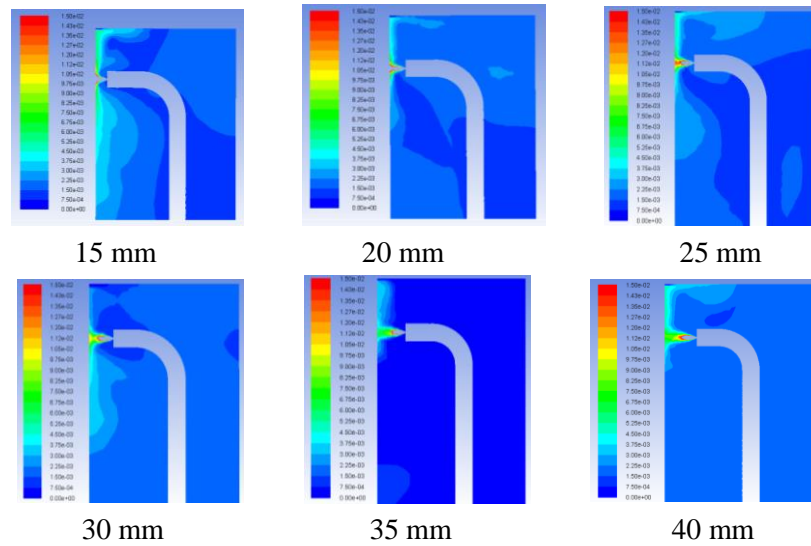


Figure 5a: Velocity field on section plane cut through spraying lance axle under 800 rpm and different standoff distances, m/s

In Fig. 5, when standoff distances are 15 mm, 20 mm and 25 mm, the velocity and water phase distribution proportion near the wall in flow field are obviously larger than those far from shell wall. The wall-attachment effect can easily be observed. For standoff distances larger than 25 mm, the velocity field still corresponds with above rule, but there exists some sparse hollow area in phase distribution. This may be caused by the air intake from inlet near the ground and the larger standoff distance.



**Figure 5b:** Phase distribution in percent (%) on section plane cut through spraying lance axle under 800 rpm and different standoff distances

Fig. 6 shows the phase distribution on ground surface under 800 rpm rotation speed and different standoff distances. The observed water phase volume proportion, which is influenced by intake air’s radial velocity and rotation speed of spraying lances, is obviously asymmetrical. If there is no influence of vacuum suction air flow, phase distribution of 4 spraying lances should be the same. But on the contrary, just because of the existing vacuum suction air flow, the whole flow field is deflected to lower right corner, where the vacuum suction port lies.

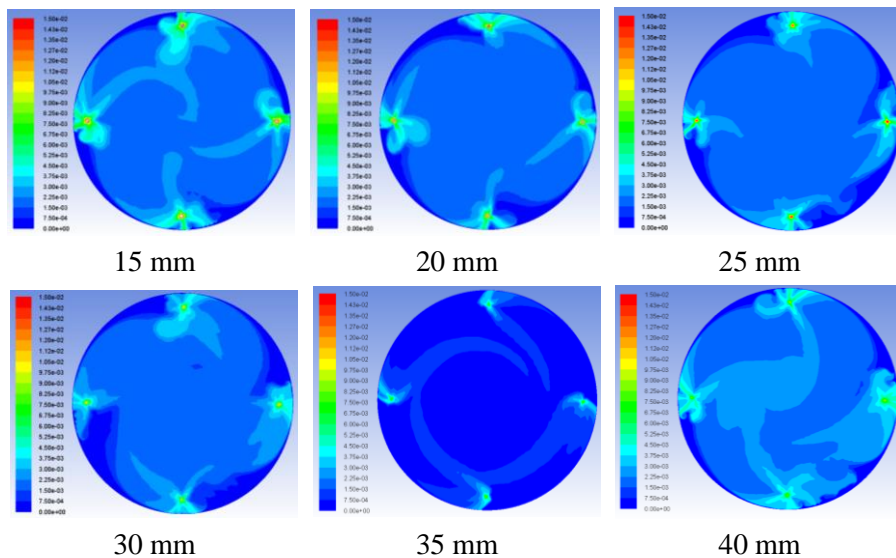


**Figure 6:** Phase distribution in percent (%) on ground 800 rpm under 800 rpm and different standoff distances

**4.2 Influence of standoff distance on cleaning ability**

After sprayed out of nozzle orifice, high speed free jet with very large Reynold number will change momentum and mass immediately with surrounding atmosphere at the turbulence interface. This will lead to undulated separation on jet's surface. With the increasing distance from orifice, the jet surface gradually becomes dispersed and disintegrated, and finally, the complete jet stream is broken into tiny liquid droplets. According to different distribution of pressure and velocity in each part, the free jet can be divided into initial section, basic section and exhausted section.

Normally, the highest pressure and fastest velocity in initial section make the pressure on stagnation point generated by waterjet impacting easy to exceed the yield and collapse strength limit of target material, so the initial section of jet is often used for waterjet cutting. While in basic section, the pressure on stagnation point is relatively smaller and cannot reach the collapse strength limit of target material, but is easier to exceed bond strength between base material and substances adhered on surface. This characteristic makes the basic section suitable for cleaning and rust removing, because the stain adhered can be cleaned without any damage to base material.

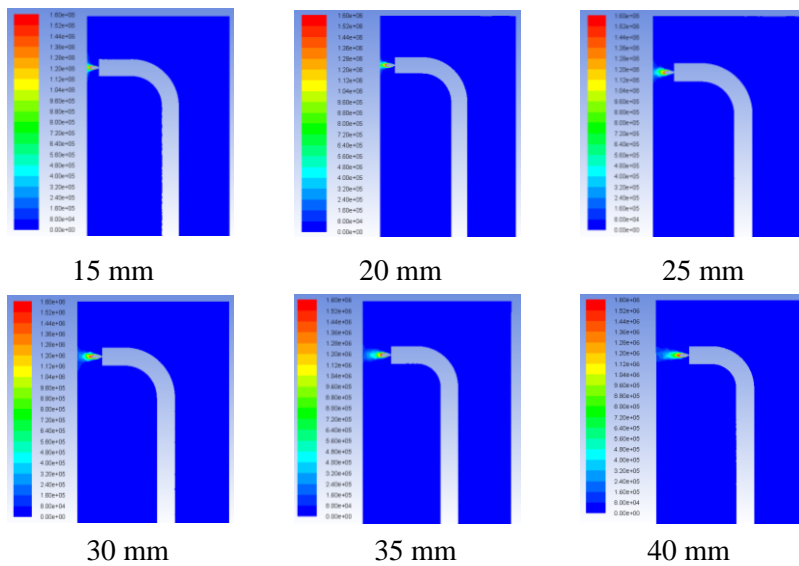


**Figure 7:** Pressure field on section plane cut through spraying lance axle under 800 rpm and different standoff distances, Pa

Fig. 7 shows pressure field in Pa on section plane cut through spraying lance axle under 800 rpm rotation speed and different standoff distances. In Fig. 7, the smaller the standoff distance is, the larger maximum pressure on ground can be seen. And this is in accordance with the experiences.

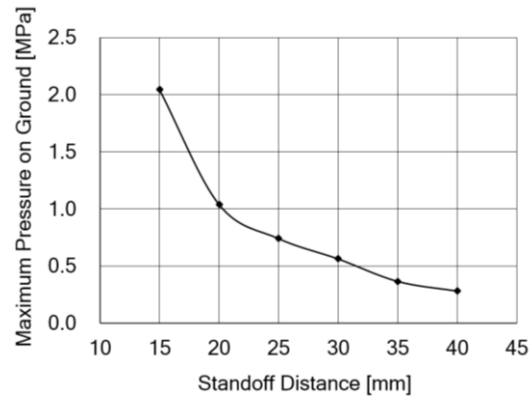


**Figure 8:** Maximum pressure on ground under 800 rpm and different standoff distance

Fig. 8 shows the maximum pressure in MPa on ground under 800 rpm rotation speed and different standoff distances, which is extracted from the different flow fields listed in Fig. 7. The curve in Fig. 8 directly reflects the relationship between maximum pressure on ground and standoff distance. From Fig. 8, we can see that the maximum pressure on ground is greatly influenced by the standoff distance. When standoff distance is varied from 15 to 30 mm with two times expansion, the maximum pressure on ground is reduced to nearly 27.45% that of 15 mm distance. This shows that the standoff distance is one of the crucial factors influencing waterjet cleaning ability.

It is required that the flexural-tensile strength for runway surface should be not less than 4.5 MPa according to “Specifications for Airport Cement Concrete Pavement Design” [MH/T 5004-2010], and the corresponding cement’s strength grades are 42.5 MPa and 52.5 MPa. Since the tensile strength of cement concrete is only 1/10 to 1/20 of its compressive strength, the concrete tensile strength can be calculated and lies between about 1.8 to 1.9 MPa [MH/T 5004-2010]. If stagnation pressure at striking point exceeds this limit, the concrete runway surface has the possibility to be damaged and tiny dents will be generated. Besides, researches carried out by Zha et al. [Zha (2015); Xie (2015)] indicate that among the three fracture mechanisms of rubber under high pressure waterjet, which are crack propagation mechanism, cavitation mechanism and stress wave mechanism, the cavitation mechanism holds predominant position. Li [Li (2009)] researched the relationship of impact pressure on target surface by cavitation waterjet to that of continuous waterjet. Result is shown as following Eq. 6:

$$P = (8.6 \sim 124) P_s \quad (6)$$

Where  $P$  is the impact pressure generated by cavitation waterjet, MPa;  $P_s$  is the impact pressure generated by continuous waterjet, MPa.

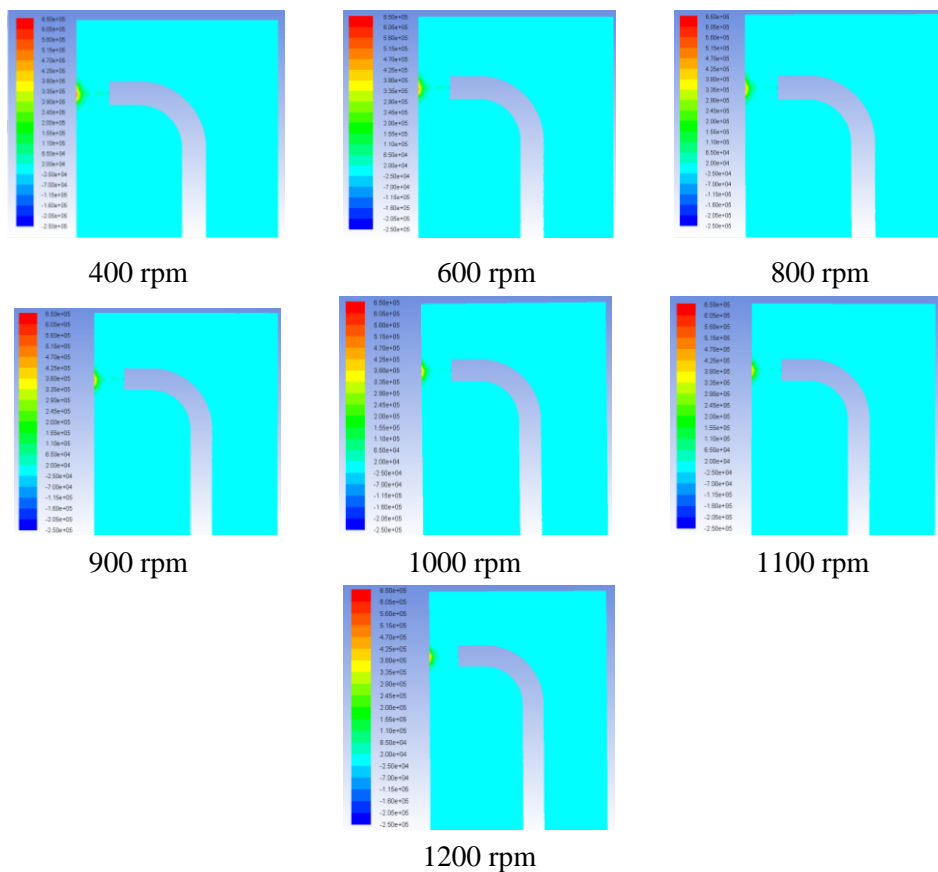
In this simulation, jet is a continuous solid stream just flowing out of nozzle orifice. But the supersonic jet stream will be surely broken after exchanging momentum and energy with surrounding air and this broken jet inevitably contains some bubbles in it. Thus an unmatured cavitation jet is formed. According to Eq. (6), considering the 4.5 MPa designed flexural-tensile strength for runway concrete and smaller amplified factor, if the stagnation pressure at striking area exceeds 0.4~0.5 MPa, the solid waterjet will possess

the ability to damage the runway surface after rubber mark adhered is removed.

In Fig. 7 and Fig. 8, when standoff distance is 15 mm and 20 mm, the maximum stagnation pressures all exceed 1 MPa, which shows obvious inapplicability. To the rest two standoff distances 25 mm and 30 mm, from Fig. 7 we can find out that width of area with stagnation pressure greater than 0.4 MPa under 30 mm standoff distance is about 80% size of spraying lance's diameter which is about 18 mm. At the meantime, the same width under 25 mm standoff distance is only 40% size of spraying lance's diameter, 9 mm. Compared between these two working conditions, cleaning under 30 mm standoff distance has the advantages of higher efficiency and doing no harm to runway surface, so it is preferable.

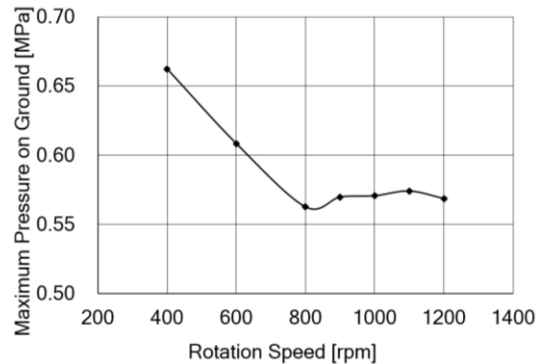
#### 4.3 Influence of rotation speed on cleaning ability

Fig. 9 shows pressure field on section plane cut through spraying lance axle under 30 mm standoff distance, different rotation speeds and same scale. The phenomenon that the maximum pressure on ground is decreased along with the increased rotation speed of spraying lances can be seen in Fig. 9 and explained by the influence of enlarged actual trajectory distance and striking angle.



**Figure 9:** Pressure field on section plane cut through spraying lance axle under 30 mm standoff distance and different rotation speeds, Pa

Fig. 10 gives the maximum normal pressure on ground under 30 mm standoff distance and different rotation speeds, whose data are extracted from the flow fields shown in Fig. 9. In Fig. 10, when spraying lances rotate from 400 rpm to 800 rpm, normal pressure on ground caused by waterjet impacting can be seen decreasing along with rising rotation speed. After 800 rpm rotation speed, the normal pressure remains steady with slight fluctuation. So, when the rotation speed is within range of below 800 rpm, the maximum normal pressure on ground is influenced greatly by the rotation speed under condition of the standoff distance remaining the same. Beyond that range, the maximum normal pressure on ground can be regarded as independent to lances' rotation speed in this simulation.



**Figure 10:** Maximum normal pressure on ground under 30 mm standoff distance

Failure criterion for brittle material is normally the strength criterion. When stress born by this kind of material reaches or exceeds its strength limit, brittle fracture occurs and material is failed. But for elastoplastic material such as rubber, fracture is normally hard to happen even if the stress endured reaches or exceeds its yield strength, and only the elastoplastic deformation can be seen. So, the maximum normal stress criterion for brittle material failure judgement is not fit for rubber. Here, the failure criterion for rubber can be considered from strain, which is that the material will fail if the maximum principal strain in either direction within material reaches its monodirectional compressive or tensile failure limit [Xie (2015)].

When high speed waterjet striking on rubber mark adhered on runway surface, maximum stagnation pressure at impacting point is not very high. As shown in Fig. 9, the value 0.66 MPa of maximum normal pressure under 30 mm standoff distance and 400 rpm rotation speed is far below the rubber's yield strength limit and breakage limit. There are three orders of magnitude. But actual cleaning operation proves that cylindrical nozzle working under 70 MPa pressure can clean runway concrete surface relatively neatly. The runway surface will be possibly damaged if slowing down the cleaner's movement velocity under this condition. From this point, mechanism for high pressure waterjet cleaning rubber mark on runway surface surely complies with the maximum shear strain criterion.

When high speed waterjet impacts on rubber mark, compressive stress is produced in rubber layer. Then a downward deformation is caused by this stress, which can generate shear stress and strain in adhered thin rubber layer. If the maximum shear strain at certain

point in rubber layer reaches its failure limit (Airplane’s tires are usually made of isoprene rubber), the adhered rubber layer is cleaned away from runway surface. From above cleaning procedure, we can draw a conclusion that the exterior rubber layer is relatively easy to clean, while the rubber layer close to runway surface is harder to clean because their deformation abilities are diverse and poor. This is also testified by actual cleaning operation.

Striking force of waterjet is gained from its momentum, which can be calculated through momentum theory. So the higher the jet’s speed is, the greater the striking force is produced. But in this kind of surface cleaner, the actual jet speed hitting on runway surface is synthesized by speed of jet itself and tangential speed component of rotation. When working pressure remains steady, the jet velocity keeps unchanged. In this instance, it seems the higher rotation speed is helpful to increase shear stress and strain in rubber layer and have better cleaning effect. But in fact, along with the rising rotation speed, waterjet trajectory from nozzle outlet to actual striking point is also enlarged. If this actual standoff distance is far beyond the optimal standoff distance which is calculated by previous researchers and 5 to 26 times the orifice diameter, the waterjet striking force will decrease instead and cleaning effect is depressed also. The reason lies in that the excessively long standoff distance causes waterjet diffusing severely by the surrounding air entrainment and dispersion.

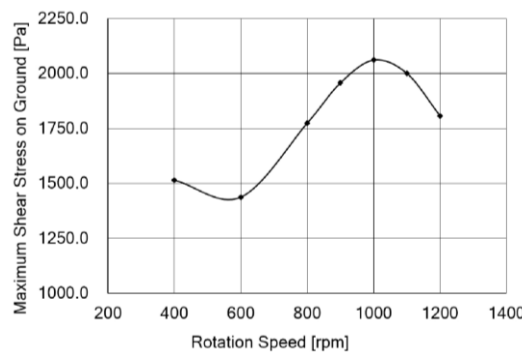


**Figure 11:** Maximum shear stress on ground under 30 mm standoff distance

Fig. 11 shows the maximum shear stress on ground caused by waterjet impacting under 30 mm standoff distance and different rotation speed. In Fig. 11, when rotation speed of lances is increased from 400 rpm, the maximum shear stress on ground first decreases and then increases to a climax. The first decreasing may be caused by the air diffusion during rotation. After that stage, the larger rotation speed finally brings a larger tangential speed to waterjet and the total striking velocity of waterjet is increased, which causes the shear stress on ground increased. Beyond the maximum limit, though it seems that the total striking velocity of waterjet should be increased along with the rising rotation speed, but in fact, if the actual waterjet trajectory from nozzle outlet to striking point is enlarged to a crucial extent, the waterjet will be shattered to water droplets by the surrounded air and its cleaning ability will be decreased.

At the meantime, as shown in Fig. 11, shear stress on ground by waterjet striking starts growing after initial slight fluctuation, reaches its climax at the rotation speed of 1000

rpm and decreases after 1000 rpm. The total curve appears to be a unimodal one, there should have a best rotation speed corresponding to maximum shear stress, which is 1000 rpm in this simulation.

## 5 Conclusion

In this paper, the actual surface cleaner used in airport runway rubber mark removing vehicle is modelled and numerically simulated. Results show that great deformation of high speed rotation waterjet flow field in semi enclosed chamber under vacuum suction is brought forth compared with that of static flow field previously studied in shape, velocity and phase distribution. Varied standoff distance and rotation speed can all influence waterjet cleaning effects. To the studied surface cleaner, 30 mm standoff distance and 1000 rpm rotation speed are relatively ideal operation parameters.

**Acknowledgement:** Many thanks should be given to Mr. Dejun Liu and Hefei Xingliang Machinery Co., Ltd., who provided many helps in this research, including supplying CAD files and measuring operation conditions during their project to supply a high pressure waterjet airport runway rubber cleaning vehicle to Beijing Airport Cleaning Co., Ltd.

## References

- Anglani, F.; Barry, J.; Dekkers, W.** (2017): Development and validation of a stationary water-spray cleaning system for Concentrated Solar Thermal (CST) reflectors. *Solar Energy*, vol. 155, pp. 574-583.
- Chen, Y. L.** (1991): *Turbulence model*. Press of University of Science and Technology of China.
- Code of Design of Concrete Structure. GB 50010-2010.
- Fu, S. C.; Dong, L. D.; Yuan, H. X.** (2014): Numerical simulation and analysis of velocity field in horizontal screw centrifuge based on euler multiphase model. *Chemical Industry and Engineering Progress*, vol. 33, pp. 36-42.
- Guo, L. J.** (2002): *Dynamics of two-phase and multi-phase flow*. Xi'an JiaoTong University Press.
- Han, Y.; Li J. C.** (2012): Selection of fluid jet nozzle under vacuum based on fluent simulation and analysis. *Vacuum*, vol. 49, pp. 19-23.
- Kummitha, O. R.** (2017): Numerical analysis of hydrogen fuel scramjet combustor with turbulence development inserts and with different turbulence models. *International Journal of Hydrogen Energy*, vol. 42, pp. 6360-6368.
- Labus, T. J.** (1995): *Fluid jet technology: fundamentals and applications*. WJTA.
- Leu, M. C.; Meng, P.; Geskin, E, S.; Tismeneskiy, L.** (1998): Mathematical modeling and experimental verification of stationary waterjet cleaning process. *Manufacturing Science Engineering, Trans ASME*, vol. 120, no. 3, pp. 571-579.
- Li, F.** (2009): *Study on vessel cleaning technology of cavitation waterjet*. Harbin Engineering University.

**Li, J. Y.; Xue, S. X.; Zhou, Q. Y.** (2007): Numerical simulation of ultra-high pressure pure water jet rust removal machine. *Engineering Journal of Wuhan University*, vol. 40, pp. 48-57.

**Li, W. Y.; Wang, J.; Zhu, H. T.; Huang, C. Z.** (2013): On ultrahigh velocity micro-particle impact on steels-a single impact study. *Wear*, vol. 305, pp. 216-227.

**MH 5010-1999**, Specifications for asphalt concrete pavement design of civil airports.

**MH/T 5004-2010**, Specifications for airport cement concrete pavement design.

**Sharif, M. A. R.; Guo, G.** (2007): Computational analysis of supersonic turbulent boundary layers over rough surfaces using the  $k-\omega$  and the Stress- $\omega$  models. *Applied Mathematical Modelling*, vol. 31, pp. 2655-2667.

**Summers, D. A.** (1995): *Waterjetting technology*. E & FN SPON.

**Sun J. J.** (1992): *Waterjet cutting technology*. Press of China University of Mining and Technology.

**Tikhomirov, R. A.; Babanin, V. F.; Petukhov, E. N.; Starikov, I. D.; Kovalev, V. A.** (1992): *High-Pressure JetCutting*. ASME.

**Welker, R.; Nagarajan, R.; Newberg, C.** (2005): Getting clean parts and getting parts clean. *Contamination and ESD Control in High-Technology Manufacturing*. pp. 195-275.

**Xie, R. T.** (2015): *Fracture mechanism of waste radial tyre rubber under ultra-high pressure water jet impact*. Hefei University of Technology.

**Yang, G. L.; Zhou, W. H.; Liu, F.** (2008): Flow field simulation of high pressure waterjet nozzle based on fluent. *Journal of Lanzhou University of Technology*, vol. 34, pp. 49-52.

**Zha, H.** (2015): *Cavitation and desulfurization mechanism of ground tire rubber under ultra-high pressure water jet impacting radial tire*. Hefei University of Technology.